



Wafer-scale epitaxy of transition-metal dichalcogenides with continuous single-crystallinity and engineered defect density

Mariam Hakami, Chien-Chih Tseng, Kohei Nanjo, Vincent Tung,*^{ORCID} and Jui-Han Fu*

Research on electronic channel materials has traditionally focused on bulk and nanocrystals, nanowires, and nanotubes. However, the recent surge of interest in two-dimensional (2D) transition-metal dichalcogenides (TMDs) has emerged as a game-changer in this field. The atomically thin structure of 2D TMDs offers unique electronic and optical properties, which have been shown to have significant potential in various applications, such as optoelectronics, energy harvesting, and spintronics. Epitaxy growth of single-crystal 2D TMDs on oxide or metallic substrates has opened up new opportunities for direct integration into existing manufacturing pathways. In this article, we discuss recent advances in achieving continuous single-crystallinity of 2D TMDs on oxide and metallic substrates by controlling the nucleation and growth rate of crystalline domains. We also review strategies for the controlled introduction of defects through postgrowth processing and substrate engineering. Finally, we highlight emerging strategies, new opportunities, and remaining challenges for bridging the gap between lab innovations and commercialization. The ability to grow high-quality 2D TMDs on scalable and industry-compatible substrates represents a significant breakthrough in the field of electronic materials and has the potential to revolutionize the semiconductor industry. Despite the remaining challenges, the future of 2D TMDs looks promising. Their integration into existing manufacturing pathways could open up new avenues for advanced electronic devices with improved performance and reduced power consumption.

Introduction

Two-dimensional (2D) transition-metal dichalcogenides (TMDs) have emerged as tantalizingly promising materials for the next generation of high-performance technology. These materials have a wide range of potential applications in fields such as electronics, photonics, and computing by virtue of their high carrier mobility and tunable bandgaps. To realize the full potential of 2D TMDs, it is essential to produce high-quality, large-scale single-crystal films. Such films would allow for their integration with silicon (Si)-based electronics, enabling the optimization for better performance. Obtaining large-area single-crystal growth of 2D TMDs involves seamlessly stitching together tens of millions of 2D domains that are all aligned in the same direction. This can be accomplished

by using a single crystalline substrate and ensuring that the lattices of the 2D materials and underlying substrates are well matched. One feasible approach to achieve this is through epitaxy, which allows for controlling the orientation of 2D TMD domains during their nucleation. In traditional epitaxy growth, the epilayer of three-dimensional (3D) materials interacts covalently with the substrate due to the existence of dangling bonds on the surfaces, and strong chemical bonding forms at the interface, which determines the orientation of the epitaxial layer. Thus, a lattice mismatch of less than 5–10% is required to achieve conventional epitaxy. On the contrary, the van der Waals (vdW) epitaxy of TMD materials results in weak interaction due to the lack of surface dangling bonds. Consequently, TMDs whose lattices have threefold symmetry

Mariam Hakami, Department of Chemical System Engineering, School of Engineering, The University of Tokyo, Tokyo, Japan; mariam_h@chemsys.t.u-tokyo.ac.jp
Chien-Chih Tseng, Department of Chemical System Engineering, School of Engineering, The University of Tokyo, Tokyo, Japan; tseng-chien-chih1982@g.ecc.u-tokyo.ac.jp
Kohei Nanjo, Department of Chemical System Engineering, School of Engineering, The University of Tokyo, Tokyo, Japan; k_nanjo@chemsys.t.u-tokyo.ac.jp
Vincent Tung, Department of Chemical System Engineering, School of Engineering, The University of Tokyo, Tokyo, Japan; vincent@g.ecc.u-tokyo.ac.jp
Jui-Han Fu, Department of Chemical System Engineering, School of Engineering, The University of Tokyo, Tokyo, Japan; fu@chemsys.t.u-tokyo.ac.jp

doi:10.1557/s43577-023-00598-1

grow antiparallel domains and thus the twin boundaries when the domains stitch with each other. The antiparallel domain formation is due to the binding energy degeneracy, and only when it is broken can the unidirectionally aligned domains be grown. Step-guided epitaxy was proposed to overcome energy degeneracy, where the edge of the step along the specific direction on the substrate acts as preferential nucleation sites that would guide the unidirectional alignment of 2D materials at a large scale.

Epitaxy of 2D TMD wafers with continuous single crystallinity

Single-crystal 2D TMDs on oxide substrates

The large-scale growth of single-crystal TMD films on insulating oxide substrates (e.g., SiO_2 , TiO_2 , and Al_2O_3) is essential for developing next-generation ultrathin and flexible electronic and optoelectronic devices. Among the oxide substrates, large-scale growth of 2D TMDs on SiO_2 substrates would enable batch fabrication and seamless integration of atomically thin high-performance transistors, memories, and phototransistors on Si-based devices without film transfer. However, the amorphous nature of SiO_2 makes it difficult to achieve epitaxial growth, which requires meticulous symmetry and lattice matching between epilayers and growth substrates. The result is the formation of small and randomly oriented TMD domains that are less than ideal for industrial scaling. Despite strenuous efforts, the size of single-crystalline MoS_2 domains on SiO_2 remains limited.^{1,2} On the contrary, when 2D TMDs are grown on insulating oxide substrates (typically single crystal in nature), the domain's shapes and orientations can be engineered by their epitaxy interaction with the underlying substrate.³ Such crystalline oxide substrates thus are employed for growing 2D TMDs, in addition to their relatively high thermal stability, chemical inertness, and atomically flat surface. These unique material properties facilitate precursor migration during chemical vapor deposition (CVD), thereby improving the thickness uniformity of the resulting 2D TMD film. For example, single-crystal strontium titanate (SrTiO_3) and titanium dioxide (TiO_2) substrates have been used for TMD growth as shown in **Figure 1**.⁴⁻⁶ Meanwhile, C-plane sapphire ($\alpha\text{-Al}_2\text{O}_3$ (0001)) has been utilized as a substrate for wafer-scale epitaxy growth of monolayer single-crystal films due to its comparable lattice constant with TMDs. Despite recent advancements in orientation control, most synthesized

films still exhibit two-directional or antiparallel domains, mainly due to the noncentrosymmetric C_{3v} lattice of TMDs. To achieve parallel domains for coalescence into a single-crystal film on most high-symmetry surfaces requires breaking energy degeneracy. Our group and Wang et al. discovered that creating parallel atomic steps through annealing simultaneously reduces surface symmetry and breaks the formation energy degeneracy of antiparallel domains.^{7,8} This led to the first demonstration of the epitaxial growth of single-crystal 2-in. monolayer MoS_2 on a miscut orientation toward the A axis (C/A) of the sapphire substrate, which is perpendicular to the standard substrates C-plane sapphire (see **Figure 2**). It was found that despite the change of miscut orientation, the formation of step edges disrupted the nucleation energy degeneracy of the antiparallel MoS_2 domains, giving rise to over 99% unidirectional growth.⁷

On the contrary, unidirectional nucleation is clearly absent in the C/M sapphire, which is defined by the major miscut angle toward the M axis with $\alpha_M \approx 0.2^\circ$ and $\alpha_A \approx 0^\circ$ (miscut angle between the (0001) plane and the substrate surface along M axis $\langle 10\bar{1}0 \rangle$), producing steps along $\langle 11\bar{2}0 \rangle$). The epitaxial relationship of the C/M substrate determines that the $\langle 11\bar{2}0 \rangle$ orientation is perpendicular to the zigzag (ZZ) edges of the triangular TMD domains and aligned with the armchair (AC) edges such as AC-1 and AC-2 in **Figure 3a-b**. These two armchair edges have similar formation energies, thus leading to the equalization of the two antiparallel domains and impeding the growth of single-crystal TMDs. To circumvent the energetic degeneracy, Wang et al. custom-designed C/A sapphire wafers, with surface steps along $\langle 10\bar{1}0 \rangle$, allowing ZZ-edge attachment and nucleation at the step predicted by the DFT calculations. Under S-rich conditions, the Mo_{ZZ} edges with the lowest formation energy (represented as ZZ-Mo-S₂ in **Figure 3b**) ensure the unidirectional growth of TMDs.⁷ Statistical analysis from multiple growths across a 2-in. wafer showed very reproducible unidirectional alignment greater than 99% on the C/A sapphire (See **Figure 3c**). In addition, a recent report on wafer-scale single-crystal TMDs dual-coupling-guided growth mechanism was conducted on vicinal A-plane sapphire ($\alpha\text{-Al}_2\text{O}_3$ with a cutting angle as small as 0.1° along a certain direction). The parallel atomic steps were formed after annealing the sapphire to break the C_2 symmetry of the A-plane sapphire.⁸ In **Figure 4a**, AFM measurement shows the longest edge of the WS_2 domain that is along the $\langle 1\bar{1}00 \rangle$ direction of sapphire

instead of along the step-edge direction of $\langle 1\bar{1}01 \rangle$. In this light, unidirectional growth is not only dominated by step-guided growth. DFT calculation further indicates that the coupling effect between A-plane sapphire and WS_2 is stronger than other

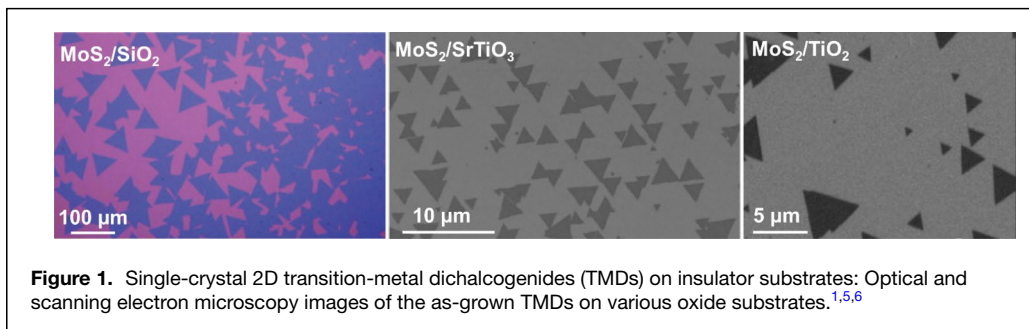


Figure 1. Single-crystal 2D transition-metal dichalcogenides (TMDs) on insulator substrates: Optical and scanning electron microscopy images of the as-grown TMDs on various oxide substrates.^{1,5,6}

insulator substrates.⁸ Therefore, antiparallel domain growth is more favorable. With the influence of the substrate step-edge, the symmetry of the substrate changes from C_2 to C_1 (lower symmetry), making it possible to have all the WS_2 islands aligned only along one direction (in this case, 60° oriented domains; see Figure 4b). However, to achieve perfect domain stitching and further high-quality single-crystal films on the sapphire substrate, careful control of the growth kinetics such as precursor concentration is key. It determines the different

types of edge structures that appeared alternately when the reaction environment changed from Mo-rich to S-rich environments, consequently, changing the docking behavior on the step of the substrate, which affects the film crystallinity.

Although there are fewer studies on directly synthesizing one-dimensional (1D) nanoribbons made from TMDs compared to the synthesis of 2D TMDs, this is mainly due to the difficulties involved in preparing, manipulating, and investigating these narrow and atomically thin crystals. However, 1D TMD nanoribbons

exhibit edge-dependent magnetic properties, lateral confinement effects, and a large surface area, making them highly tunable and, therefore, a promising platform for advanced applications such as magnetoresistive devices or catalyst application. The process of growing 1D TMDs has been closely studied. Our group reported the self-aligned

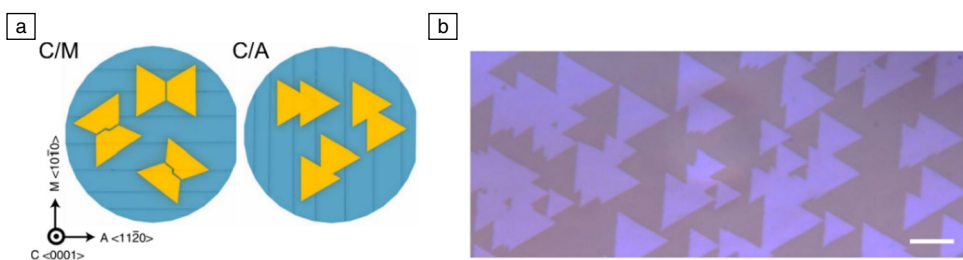


Figure 2. C/M and C/A sapphire (0001) substrate and epitaxial relationship. (a) Step orientations on C/M (a) and C/A (d) sapphire (0001) wafers and the corresponding epitaxial MoS₂ domain alignment.⁷ (b) Optical microscopy image of MoS₂ domains grown on a C/A ($\alpha_A = 0.89^\circ$) substrate. Scale bar = 10 μm.⁷

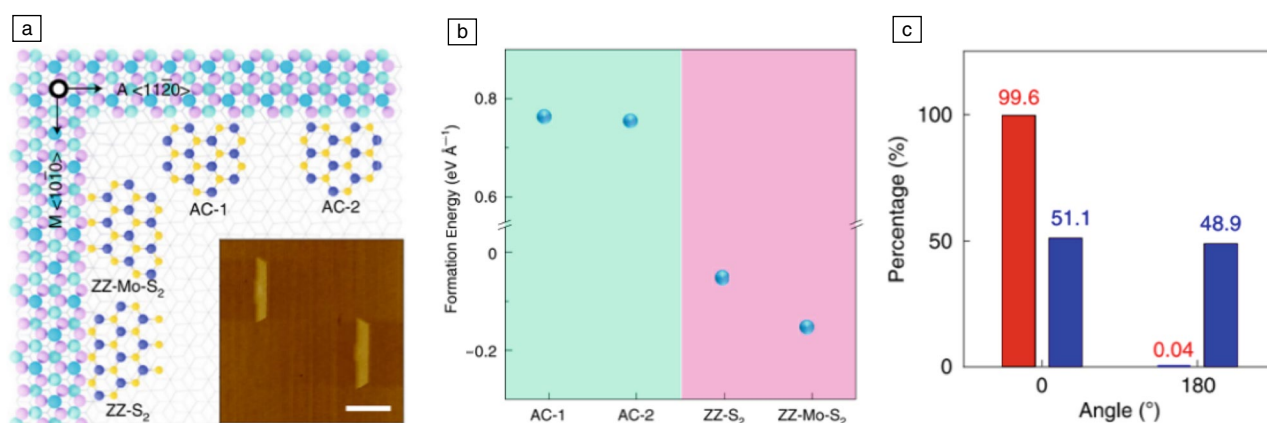


Figure 3. C/M and C/A sapphire (0001) substrate and epitaxial relationship. (a) Four possible edge configurations during the nucleation stage on the C/A and C/M substrates. Inset: Atomic force microscope image of a sample at the early growth stage, showing that the nucleation is along the step edges. Scale bar = 500 nm.⁷ (b) The calculated formation energy of the four edge configurations.⁷ (c) Statistical distribution of antiparallel domains on C/A (red) and C/M (blue) substrates.⁷

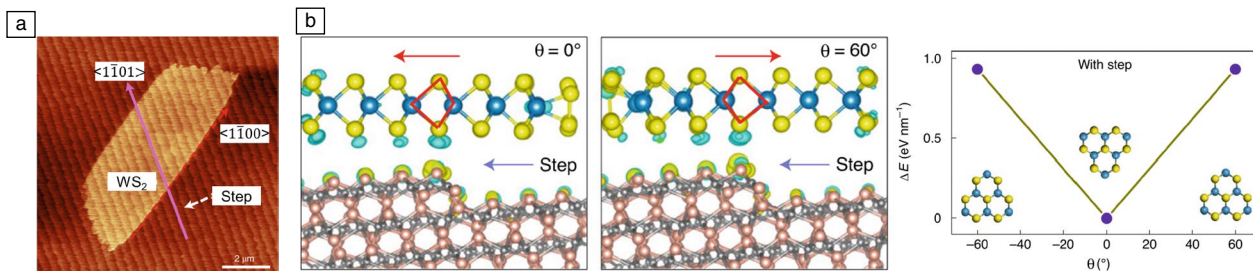


Figure 4. Characterization of WS_2 islands and dual-coupling-guided epitaxial growth on vicinal A-plane sapphire. (a) Atomic force microscopy image of WS_2 domain on A- Al_2O_3 . The direction of the Al_2O_3 steps is $\langle 1\bar{1}01 \rangle$.⁸ (b) Left: Optimized structures of antiparallel WS_2 ribbons crossing an atomic step of A-plane sapphire (side view) for $\theta = 0^\circ$ and $\theta = 60^\circ$. Right: Relative energy difference between two antiparallel WS_2 islands that cross a step edge on the A-plane sapphire surface due to symmetry breaking.⁸

growth of monolayered TMD nanoribbons on ledge-structured β - Ga_2O_3 . The atomically sharp steps on the freshly exfoliated (100) plane create two sets of structurally equivalent but crystallographically inverted ledges (001 and -201), breaking the symmetry and serving as a template for the growth of MoS_2 nanoribbons along a single direction. We further utilized the ledge-directed growth method as the generalized growth platform to afford single-crystal TMD nanoribbons and their lateral- and vertical heterostructures. Recently, the uniformly aligned single-crystal TMD ribbons through edge epitaxial growth mode are also validated on high-Miller-index Au facets (see **Figure 5**).^{9,10}

Single-crystal 2D TMDs on metallic substrate

Despite potential contaminations or difficulty in subsequent device fabrication processes, synthesizing 2D TMDs on conductive surfaces can leverage compatibility with direct atomic-scale characterizations. Au(111) is mainly the metal substrate used for its chemical inertness for sulfur vapor.^{10–12} Its matched lattice symmetry with TMD materials and the interface coupling between Au and TMDs is stronger than insulator substrates,¹¹ facilitating the epitaxial growth of 2D layered materials toward wafer-scale single crystals. Melting and resolidifying the metal at high temperatures is a technique for obtaining an atomically flat surface for monolayer deposition and forming a single-crystal Au(111) surface.¹³ Most importantly, under such high-temperature annealing, atomic steps are periodically formed on the surface. These atomic steps align with the subsequent nucleations of TMDs, resulting in unidirectional growth and subsequent merge into single-crystal growth. Theoretical models constructed by DFT calculations corroborate the step-guided epitaxial growth of TMDs on vicinal Au(111) (**Figure 6**, single-crystal growth of TMDs such as WSe_2 and MoS_2 is represented).^{10,12–14} The scanning transmission electron microscopy (STEM) image in **Figure 7a** shows one ZZ-edge of a monolayer MoS_2 domain docking along the $\langle 110 \rangle$ direction of the vicinal Au(111) surface. Moreover, there are two kinds of step edges of a terrace along the Au $\langle 110 \rangle$ direction, namely A-step and B-step, as in

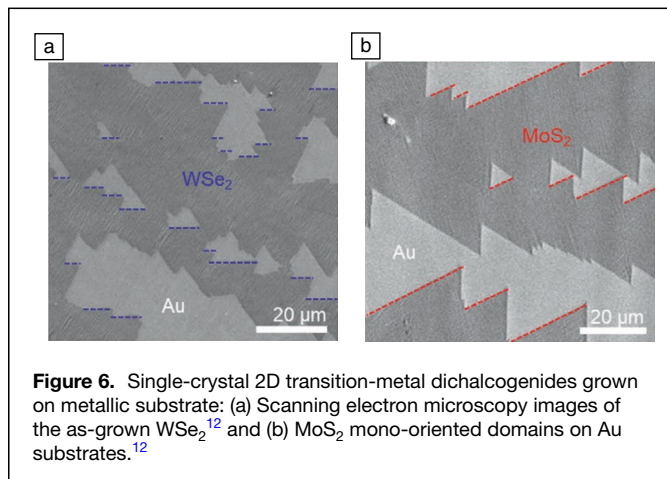


Figure 6. Single-crystal 2D transition-metal dichalcogenides grown on metallic substrate: (a) Scanning electron microscopy images of the as-grown WSe_2 ¹² and (b) MoS_2 mono-oriented domains on Au substrates.¹²

Figure 7b. The minimum energy states occur at $\theta = 0^\circ$ with the Mo_{ZZ} edge docking. The contact energies per MoS_2 unit for the step-guided epitaxy are -1.34 eV/f.u. (electron volt per formula unit) for A-step and -1.50 eV/f.u. for B-step, with a difference of 0.16 eV/f.u. The docking to the B-step is more favorable due to its higher binding energy, which is comparable to the case for h-BN/Cu(111).¹⁵ Also, the contact energies per unit length calculated for different MoS_2 edges show that the coupling between the Mo_{ZZ} edge and B-step is energetically more favorable. However, during the optimization of contacting structures, there is a special case for S_{ZZ} edges (60°) of MoS_2 docking at the A-step edge.¹³ In contrast, sulfur atoms energetically favor 0° at the step edge over other angles in the case of WS_2 (**Figure 7c**).¹²

This discrepancy sparks debates on whether the existence of steps on the surfaces truly underpins the unidirectional nucleation and, thus, the single-crystal growth of TMDs. Hence, to ensure single-crystal film growth on the Au substrate, the influence of the step needs to be assisted with the precise control of precursor flux ratio as it significantly affects the alignment of MoS_2 domains on the step. Where both 0° and 60° oriented MoS_2 islands appeared at low S/Mo ratio and with an increase in the sulfur supply, 0° aligned domains became dominant. To this end, D. Ding et al. investigated the atomic-scale nucleation of TMDs on a Au(111) substrate at the early stage of the growth and its mechanism. The statistical analysis shows that most as-grown MoS_2 domains ($\sim 88\%$ and 90% for MoSe_2) nucleate on surface terraces, with 12% (10% for MoSe_2) of MoS_2 flakes docking on surface steps. In addition, most of the step-associated nucleation is $\sim 64\%$ Mo_{ZZ} -edge-terminated, and the rest are docked at S_{ZZ} -edges. The optical image in **Figure 8a** shows unidirectional nucleation on the Au surface, and the atomic structures of MoS_2 on Au(111) for terrace nucleation and step-associated nucleation are presented in the STEM images in **Figure 8b**. Admittedly, the terrace-nucleated MoS_2 domains are terminated with two free edges. At the same time, oppositely, the step-nucleated ones reside at the atom-high step edge with one side as the Mo_{ZZ} edge and the other

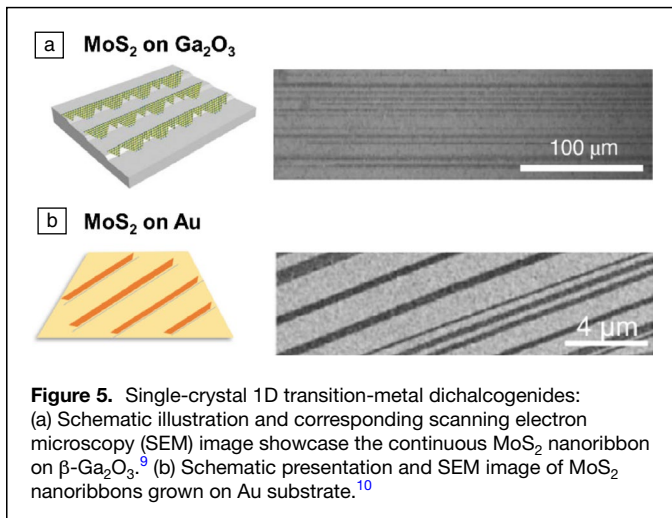


Figure 5. Single-crystal 1D transition-metal dichalcogenides: (a) Schematic illustration and corresponding scanning electron microscopy (SEM) image showcase the continuous MoS_2 nanoribbon on β - Ga_2O_3 .⁹ (b) Schematic presentation and SEM image of MoS_2 nanoribbons grown on Au substrate.¹⁰

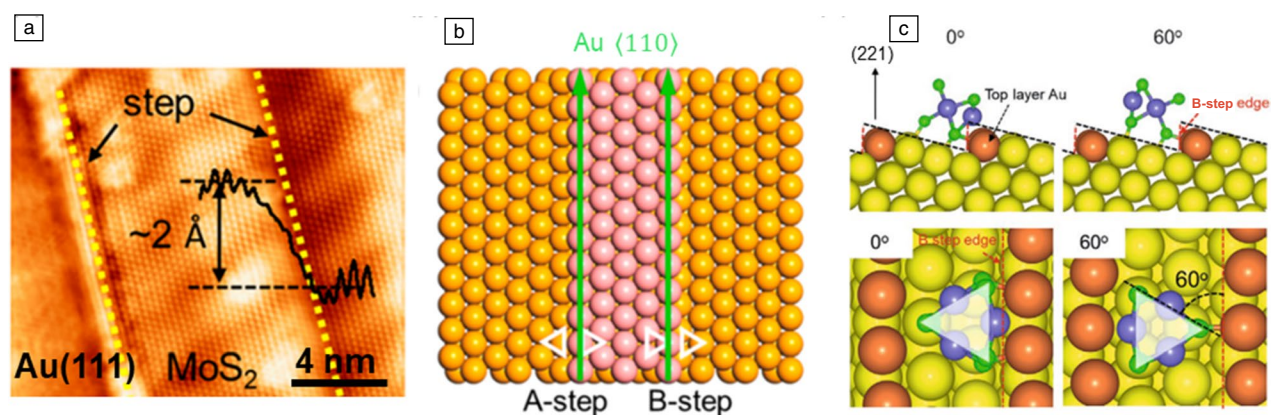


Figure 7. Theoretical calculations for the internal mechanism of step-induced growth of transition-metal dichalcogenides/Au. (a) Scanning transmission electron microscopy image of one edge of the MoS₂ domain docking with the step of Au(111).¹³ (b) Two typical step edges (A-step and B-step) along the $\langle 110 \rangle$ direction on the Au(111) surface. Atoms in pink and orange represent the stepped Au and substrate Au atoms, respectively.¹³ (c) Side and top views of the W₃S₆ cluster resided on Au(221) surface with rotation angles of 0° and 60°, respectively.¹²

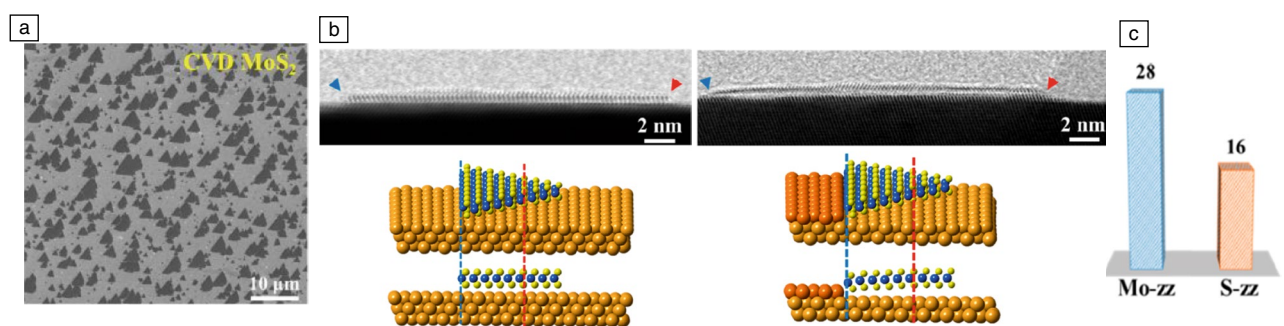


Figure 8. Cross-sectional characterization of MoS₂ domains at the nucleation stage. (a) Chemical vapor deposition (CVD)-grown MoS₂ domains scattered all over on Au(111).¹⁶ (b) Left: Scanning transmission electron microscopy (STEM) image of the interfacial structure and atomic model of MoS₂ domains nucleated on the Au terrace. Right: STEM image of the interfacial structure and atomic model of MoS₂ domains with a one-sided Mo_{ZZ} edge in contact with the Au step.¹⁶ (c) Statistical analysis of the edge structure of Mo_{ZZ} and S_{ZZ} in contact with the Au step.¹⁶

one as the free end. In alignment with DFT calculations, the results confirm that vdW terrace-nucleation, rather than the surface step-guided epitaxy, plays an essential role in realizing unidirectional TMD domains on the Au(111) substrate. Surface step heights are mainly responsible for the integrity and thickness of MoS₂/MoSe₂ films.¹⁶

Single-crystal 2D TMDs on semiconductor substrate

Using semiconductor substrates such as Si, SiC, and GaN as a foundation for synthesizing TMDs holds great promise for developing energy-efficient, high-speed, and high-power devices that combine 2D layered materials with 3D semiconductors in electronic and optoelectronic applications.¹⁷ However, the current results from these growth processes show either two distinct growth orientations (0° and 60°) on GaN or the formation of small nanocrystals with uniform width on Si(001) surfaces pretreated with phosphine. To fully utilize semiconductor substrates for large-scale production and achieve single-crystal TMDs, additional efforts and advancements are necessary.^{18,19}

TMD engineered defect density

Defects in 2D materials

The defects in CVD-synthesized TMDs can arise from several sources, including impurities in the starting materials, the growth conditions, nonuniform or incomplete reactions between the precursor molecules and the substrate surface, and postgrowth treatment. Typical defects in 2D TMDs can be classified into 0D point defects, 1D grain boundaries, and 2D stacking faults.^{20,21} Point defects can coexist within the 2D material matrix, such as substitution impurities, adatoms, antisites, and vacancies. Among them, vacancies are the most observed defects in 2D TMDs.²¹ More specifically, chalcogen vacancies are widely common in CVD-grown 2D TMDs compared to transition-metal atom vacancies.^{22,23} Taking single-layer MoS₂ as an example, one sulfur vacancy (V_{1s}), and disulfur vacancy (V_{2s}), vacancy complex of Mo and nearby three sulfur (V_{MoS3}), vacancy complex of Mo nearby three disulfur pairs (V_{MoS6}), and S₂ column substituting a Mo atom (S_{2Mo}) are commonly observed point defects under STEM (See

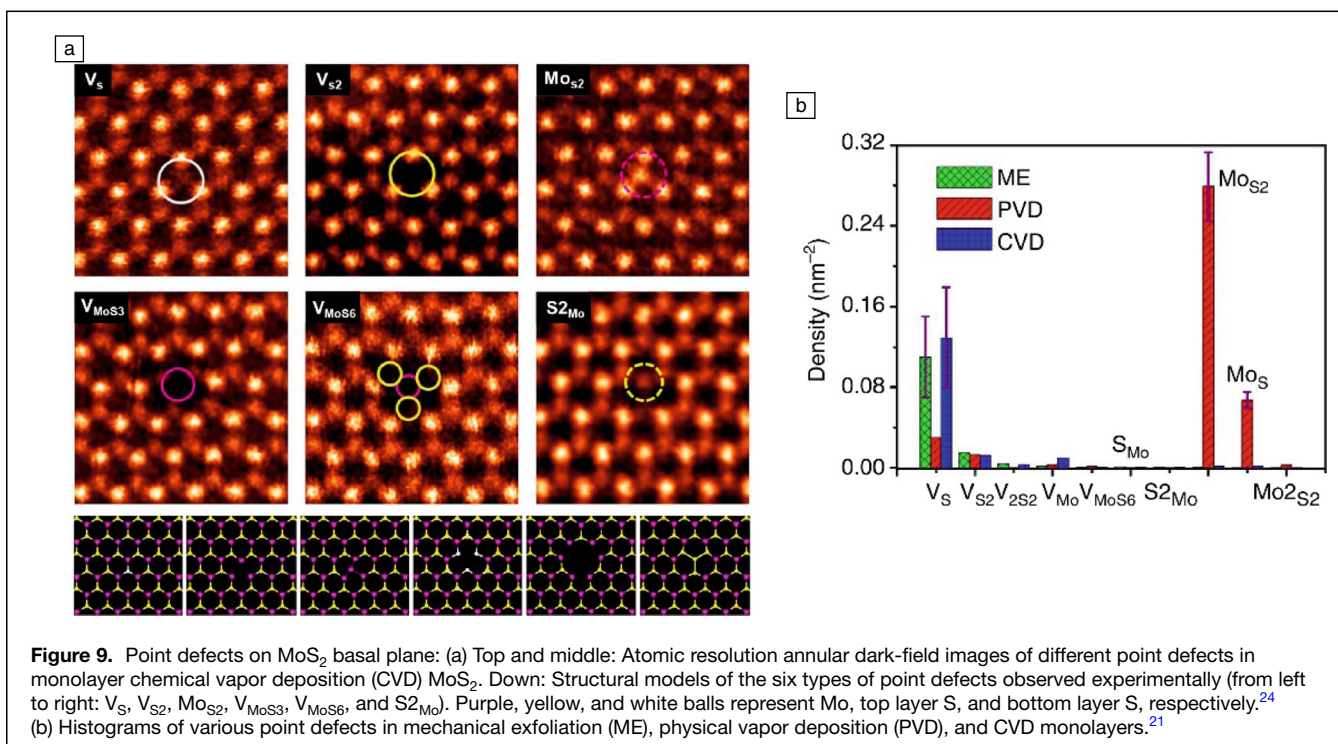


Figure 9. Point defects on MoS₂ basal plane: (a) Top and middle: Atomic resolution annular dark-field images of different point defects in monolayer chemical vapor deposition (CVD) MoS₂. Down: Structural models of the six types of point defects observed experimentally (from left to right: V_S, V_{S2}, Mo_{S2}, V_{MoS3}, V_{MoS6}, and S_{2Mo}). Purple, yellow, and white balls represent Mo, top layer S, and bottom layer S, respectively.²⁴ (b) Histograms of various point defects in mechanical exfoliation (ME), physical vapor deposition (PVD), and CVD monolayers.²¹

Figure 9a).²⁴ V_{1s} formation energy is the lowest among them according to density functional theory (DFT), where the formation energy of V_{2s} is roughly twice that of V_{1s}.^{22,23} Antisite defects of Mo and S can also be formed during the growth stage where a Mo atom substitutes a S₂ column (Mo_{S2}), or a S₂ column substitutes a Mo atom (S_{2Mo})²¹ as shown in Figure 9a. However, antisite defects are occasionally observed in CVD growth, unlike physical vapor deposition (PVD) produced samples, where antisite defects with one Mo atom replacing one or two S atoms (Mo_S or Mo_{S2}) are frequently observed (See Figure 9b).²¹ Substitution is where foreign atoms are inserted within the 2D material layer, replacing their original atom. However, when atoms get adsorbed to the surface, they form adatoms. Some causes of such adatoms or substitutions are formed during ambient exposure or impurities during epitaxy growth.²⁵

Engineering the defects in 2D materials

One major obstacle for CVD-synthesized TMDs is lacking control of the type or density of the defects. This results in undesirable doping or trapping states, thus causing unwanted charge recombination and degradation of the device performance, as well as poor luminescence quantum yields. Therefore, practical and rational engineering of defects holds significant promise for optimizing the properties of CVD-TMDs and unlocking their potential for next-generation electronic and optoelectronic devices.^{24,26} Defect density can be controlled during the synthesis stage or post-synthesis treatments. The former is mainly achieved by stoichiometry deviations or doping. In contrast, the latter can create or heal defective sites by any method, such as ion bombardment, plasma treatment,

and chemical treatment.^{27–29} Although significant progress has been reported in achieving electronic-grade TMDs with wafer-scale crystallinity, the precise control of sulfur vacancies in CVD-grown MoS₂ or WS₂ remains in its infancy. Like any material, these atomically thin 2D TMD films are not perfect. High densities of defects that are rich in variety adversely affect the field-effect carrier mobility and photoluminescence. Because the CVD method depends on reacting the volatile transition-metal oxides (e.g., MoO₃ or WO₃) with chalcogenides in the vapor phase, the key to achieving low defect density lies in a well-controlled sulfurization/selenization rate. To this end, our group has leveraged hydroxide tungsten species, an intermediate of WO₃, to effectively undergo the sulfurization while suppressing the formation of point defects during the growth stage. We found that the use of hydroxide vapor-phase deposition (OHVPD) leads to one order of magnitude lower defect density of TMDs compared to those from conventional CVD methods. Scanning tunneling microscopy (STM) measurements in **Figure 10a** show CVD-WS₂ and OHVPD-WS₂ monolayers directly synthesized on highly oriented pyrolytic graphite (HOPG) substrates. It is evident that CVD-WS₂ exhibits more structural defects than OHVPD-WS₂, which makes OHVPD a very efficient method of controlling defect density, leading to about one order of magnitude lower defect density compared to those from conventional CVD methods.³⁰ Another work conducted by Shen et al. suggested that the oxygen-incorporated CVD method for healing the donor defect states induced by sulfur vacancies in MoS₂. X-ray photoelectron spectroscopy (XPS) data show the formation of molybdenum-oxygen bonding at the sulfur vacancy sites of O-MoS₂ (see Figure 10b). The enhancement

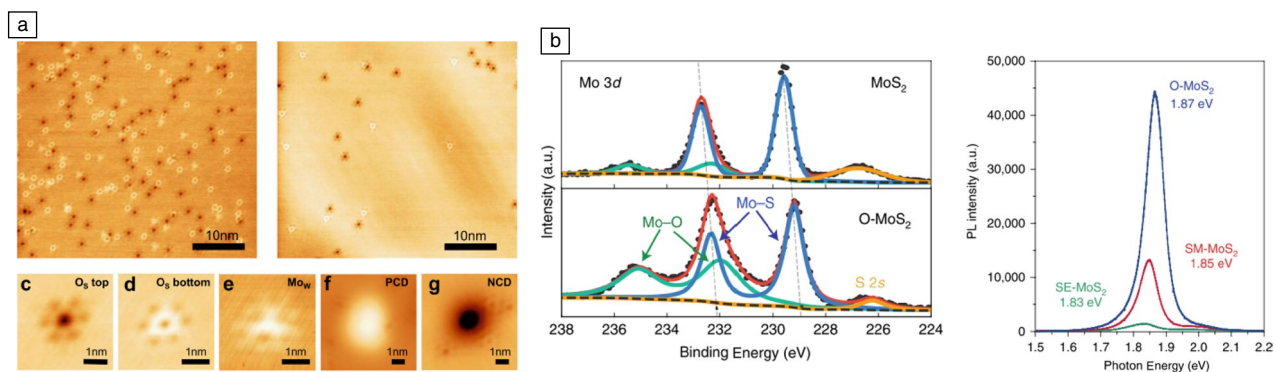


Figure 10. During-synthesis methods of engineering the defects in 2D materials: (a) Left: Scanning tunneling microscopy images of a chemical vapor deposition (CVD)-WSe₂. Right: Hydroxide vapor-phase deposition-WSe₂.³⁰ (b) Left: X-ray photoelectron spectroscopy data of Mo 3d for CVD MoS₂ and O-MoS₂. Right: Typical photoluminescence (PL) spectra of O-MoS₂, SM-MoS₂, and SE-MoS₂ on SiO₂/Si substrate showing PL enhancement of O-MoS₂.³¹

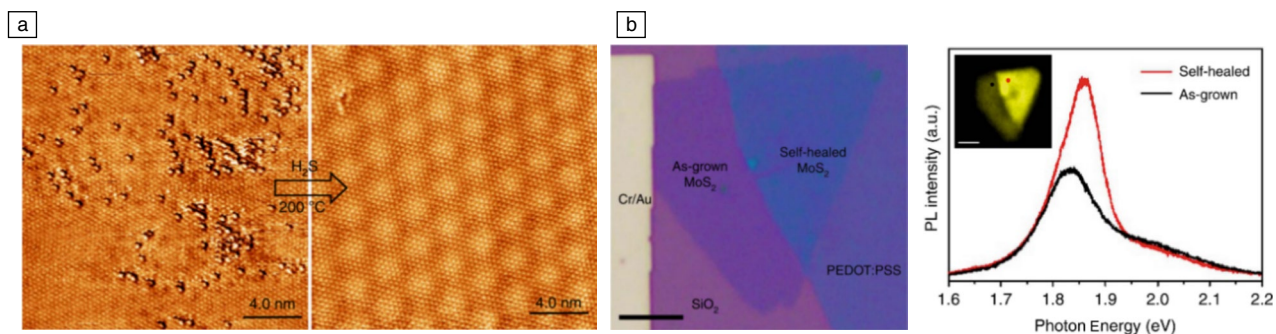


Figure 11. Post-synthesis methods of engineering the defects in 2D materials: (a) Scanning tunneling microscopy images of 2D MoS_{2-x} before (left) and after (right) 30 min. annealing at 200°C in H₂S.²⁵ (b) Left: Optical microscopy image of the as-grown and self-healed samples. Scale bar = 5 mm. Right: Photoluminescence (PL) spectra acquired from different regions are highlighted in the inset.³³

of the PL intensity and the blueshift in the PL peak position in O-MoS₂ seen in Figure 10b suggests that the neutral excitons are much more populated than trions, which is a common sign of less *n*-type doping and lower sulfur defect density.³¹

In parallel, post-synthesis treatments for vacancy healing have been explored, such as annealing of 2D TMD materials under a chalcogenide environment. In Figure 11a, atomic-resolution STM images show the monolayer 2D MoS_{2-x}O_x with oxygen substitution of sulfur vacancies after exposure to air and annealing in a hydrogen sulfide (H₂S) atmosphere at 200°C. STM results indicate that 2D MoS_{2-x}O_x crystals can be reduced to the original state of defect-free MoS₂ via efficient surface chemistry engineering.²⁵ Similar approaches, including high-pressure annealing under only a sulfur environment, show remarkable recovery of the crystal quality in MoS₂.³² Not only the dry method of gas annealing has been used, but also the wet solution treatment has been explored. As shown in Figure 11b, bilayered MoS₂ is assembled by a dry transfer. Then, self-healing of sulfur vacancies spontaneously occurs by virtue of assembling sulfur adatom clusters on the MoS₂ basal plane through a nonoxidizing acid poly(4-styrene sulfonate), thus enabling the hydrogenation process. The resulting PL spectra

indicate the restoration of the MoS₂ basal plane after the chemical treatment.³³ Moreover, plasma treatments are utilized to modify chalcogen defect concentrations in monolayer TMDs, enabling the addition of new functionalities. For instance, by controlling ion energy and sputtering time in a helium plasma, the properties of MoS₂ can be adjusted from being semiconducting to exhibiting metallic-like behavior through the introduction of S defects. Similarly, *p*-type MoS₂ can be obtained by subjecting it to oxygen plasma treatment.^{34–37}

Conclusion and outlook

To date, large-scale and single-crystal TMD monolayers have been successfully obtained on single-crystal metal or insulator substrates by the CVD method via two routes: (1) nucleation and growth of a single nucleus on a substrate and (2) the seamless coalescence of unidirectionally aligned 2D domains on a tailored substrate. Despite the tremendous efforts in achieving large-scale and high-quality CVD-TMDs and their integration into industrial fabrication and applications, the growth mechanisms, especially the nucleation of single-crystal 2D TMDs, have not been thoroughly unraveled, making precise and controllable growth difficult to achieve at large scale. Meanwhile, engineering defects

in 2D TMDs is a fascinating area for maximizing their potential. Although defects from grain boundaries can be eliminated with single-crystal growth, intrinsic vacancies still impact material quality. In-depth studies of reaction chemistries and post-synthesis treatments are crucial for defect engineering in 2D TMDs. Additionally, new or modified designs in automated CVD systems are necessary due to challenges in maintaining consistent chalcogenide-to-metal concentrations and achieving uniform deposition of evaporated molecules. This limitation makes it difficult to control defects or utilize current laboratory-scale CVD growth methods for industrial applications. Furthermore, plasma treatments offer an additional avenue for defect manipulation and functionalization in 2D TMDs, providing exciting opportunities for tailoring their properties and adding new functionalities. Collaborative efforts between academia and industry are essential to advance scalable and reliable production methods for TMDs and bridge the gap between laboratory discoveries and fabrication processes. Further advancements in the growth of 2D vertical and lateral heterostructures with high crystallinity and large scale hold significant potential for a wide range of optoelectronic and electronic devices. These advancements offer opportunities to develop high-performance logic gates and digital integrated circuits, including complementary metal oxide semiconductor (CMOS) inverters. TMD-based field-effect transistors (FETs) have already demonstrated promising characteristics, such as higher on/off current ratios and lower subthreshold swings compared to traditional silicon-based FETs. However, integrating TMDs with CMOS technology requires bridging the gap between laboratory innovations and fabrication production. This calls for collaboration between academia and industry to develop scalable and reliable production methods for TMDs.

Funding

Open access funding provided by The University of Tokyo. V.T. and J.-H.F. are indebted to the financial support from the Japan Society for the Promotion of Science (JSPS, 23H00253) and The University of Tokyo.

Conflict of interest

On behalf of all authors, the corresponding author states that there is no conflict of interest.

Open Access

This article is licensed under a Creative Commons Attribution 4.0 International License, which permits use, sharing, adaptation, distribution and reproduction in any medium or format, as long as you give appropriate credit to the original author(s) and the source, provide a link to the Creative Commons licence, and indicate if changes were made. The images or other third party material in this article are included in the article's Creative Commons licence, unless indicated otherwise in a credit line to the material. If material is not included in the article's Creative Commons licence and your intended use is not permitted by statutory regulation or exceeds the permitted use, you will need to obtain permission directly

from the copyright holder. To view a copy of this licence, visit <http://creativecommons.org/licenses/by/4.0/>.

References

1. A.M. van der Zande, P.Y. Huang, D.A. Chenet, T.C. Berkelbach, Y. You, G.-H. Lee, T.F. Heinz, D.R. Reichman, D.A. Muller, J.C. Hone, *Nat. Mater.* **12**, 554 (2013)
2. H. Yin, X. Zhang, J. Lu, X. Geng, Y. Wan, M. Wu, P. Yang, *J. Mater. Sci.* **55**, 990 (2019)
3. Q. Ji, M. Kan, Y. Zhang, Y. Guo, D. Ma, J. Shi, Q. Sun, Q. Chen, Y. Zhang, Z. Liu, *Nano Lett.* **15**, 198 (2015)
4. P. Chen, W. Xu, Y. Gao, J.H. Warner, M.R. Castell, *ACS Appl. Nano Mater.* **1**, 6976 (2018)
5. C. Huang, J. Fu, M. Xiang, J. Zhang, H. Zeng, X. Shao, *ACS Nano* **15**, 8610 (2021)
6. M. Xiang, C. Huang, Y. Xing, H. Liu, X. Shao, *ACS Appl. Nano Mater.* **5**, 7609 (2022)
7. T. Li, W. Guo, L. Ma, W. Li, Z. Yu, Z. Han, S. Gao, L. Liu, D. Fan, Z. Wang, Y. Yang, W. Lin, Z. Luo, X. Chen, N. Dai, X. Tu, D. Pan, Y. Yao, P. Wang, Y. Nie, J. Wang, Y. Shi, X. Wang, *Nat. Nanotechnol.* **16**, 1201 (2021)
8. J. Wang, X. Xu, T. Cheng, L. Gu, R. Qiao, Z. Liang, D. Ding, H. Hong, P. Zheng, Z. Zhang, Z. Zhang, S. Zhang, G. Cui, C. Chang, C. Huang, J. Qi, J. Liang, C. Liu, Y. Zuo, G. Xue, X. Fang, J. Tian, M. Wu, Y. Guo, Z. Yao, Q. Jiao, L. Liu, P. Gao, Q. Li, R. Yang, G. Zhang, Z. Tang, D. Yu, E. Wang, J. Lu, Y. Zhao, S. Wu, F. Ding, K. Liu, *Nat. Nanotechnol.* **17**, 33 (2022)
9. A. Aljarb, J.-H. Fu, C.-C. Hsu, C.-P. Chuu, Y. Wan, M. Hakami, D.R. Naphade, E. Yengel, C.-J. Lee, S. Brems, T.-A. Chen, M.-Y. Li, S.-H. Bae, W.-T. Hsu, Z. Cao, R. Albaridy, S. Lopatin, W.-H. Chang, T.D. Anthopoulos, J. Kim, L.-J. Li, V. Tung, *Nat. Mater.* **19**, 1300 (2020)
10. P. Yang, D. Wang, X. Zhao, W. Quan, Q. Jiang, X. Li, B. Tang, J. Hu, L. Zhu, S. Pan, Y. Shi, Y. Huan, F. Cui, S. Qiao, Q. Chen, Z. Liu, X. Zou, Y. Zhang, *Nat. Commun.* **13**, 3238 (2022)
11. J. Shi, X. Zhang, D. Ma, J. Zhu, Y. Zhang, Z. Guo, Y. Yao, Q. Ji, X. Song, Y. Zhang, *ACS Nano* **9**, 4017 (2015)
12. S.H. Choi, H.-J. Kim, B. Song, Y.I. Kim, G. Han, H.T.T. Nguyen, H. Ko, S. Boandoh, J.H. Choi, C.S. Oh, H.J. Cho, J.W. Jin, Y.S. Won, B.H. Lee, S.J. Yun, B.G. Shin, H.Y. Jeong, Y.-M. Kim, Y.-K. Han, Y.H. Lee, S.M. Kim, K.K. Kim, *Adv. Mater.* **33**, 2006601 (2021)
13. P. Yang, S. Zhang, S. Pan, B. Tang, Y. Liang, X. Zhao, Z. Zhang, J. Shi, Y. Huan, Y. Shi, S.J. Pennycook, Z. Ren, G. Zhang, Q. Chen, X. Zou, Z. Liu, Y. Zhang, *ACS Nano* **14**, 5036 (2020)
14. K.V. Bets, N. Gupta, B.I. Yakobson, *Nano Lett.* **19**, 2027 (2019)
15. X. Li, G. Wu, L. Zhang, D. Huang, Y. Li, R. Zhang, M. Li, L. Zhu, J. Guo, T. Huang, J. Shen, X. Wei, K.M. Yu, J. Dong, M.S. Altman, R.S. Ruoff, Y. Duan, J. Yu, Z. Wang, X. Huang, F. Ding, H. Shi, W. Tang, *Nat. Commun.* **13**, 1773 (2022)
16. D. Ding, S. Wang, Y. Xia, P. Li, D. He, J. Zhang, S. Zhao, G. Yu, Y. Zheng, Y. Cheng, M. Xie, F. Ding, C. Jin, *ACS Nano* **16**, 17356 (2022)
17. P. Wang, D. Yang, X. Pi, *Adv. Electron. Mater.* **7**, 2100278 (2021)
18. Y. Wan, J. Xiao, J. Li, X. Fang, K. Zhang, L. Fu, P. Li, Z. Song, H. Zhang, Y. Wang, M. Zhao, J. Lu, N. Tang, G. Ran, X. Zhang, Y. Ye, L. Dai, *Adv. Mater.* **30**, 1703888 (2018)
19. D. Ruzmetov, K. Zhang, G. Stan, B. Kalanyan, G.R. Bhimanapati, S.M. Eichfeld, R.A. Burke, P.B. Shah, T.P. O'Regan, F.J. Crowne, A.G. Birdwell, J.A. Robinson, A.V. Davydov, T.G. Ivanov, *ACS Nano* **10**, 3580 (2016)
20. K.-K. Liu, W. Zhang, Y.-H. Lee, Y.-C. Lin, M.-T. Chang, C.-Y. Su, C.-S. Chang, H. Li, Y. Shi, H. Zhang, C.-S. Lai, L.-J. Li, *Nano Lett.* **12**, 1538 (2012)
21. J. Hong, Z. Hu, M. Probert, K. Li, D. Lv, X. Yang, L. Gu, N. Mao, Q. Feng, L. Xie, J. Zhang, D. Wu, Z. Zhang, C. Jin, W. Ji, X. Zhang, J. Yuan, Z. Zhang, *Nat. Commun.* **6**, 6293 (2015)
22. D. Liu, Y. Guo, L. Fang, J. Robertson, *Appl. Phys. Lett.* **103**, 183113 (2013)
23. M.R. Rosenberger, H.-J. Chuang, K.M. McCreary, C.H. Li, B.T. Jonker, *ACS Nano* **12**, 1793 (2018)
24. W. Zhou, X. Zou, S. Najmaei, Z. Liu, Y. Shi, J. Kong, J. Lou, P.M. Ajayan, B.I. Yakobson, J.-C. Idrobo, *Nano Lett.* **13**, 2615 (2013)
25. J. Pető, T. Ollár, P. Vancsó, Z.I. Popov, G.Z. Magda, G. Dobrik, C. Hwang, P.B. Sorokin, L. Tapasztó, *Nat. Chem.* **10**, 1246 (2018)
26. J.H. Park, A. Sanne, Y. Guo, M. Amani, K. Zhang, H.C.P. Movva, J.A. Robinson, A. Javey, J. Robertson, S.K. Banerjee, A.C. Kummel, *Sci. Adv.* **3**, e1701661 (2017)
27. S. Bertolazzi, S. Bonacchi, G. Nan, A. Pershin, D. Beljonne, P. Samori, *Adv. Mater.* **29**, 1606760 (2017)
28. Z. Yu, Y. Pan, Y. Shen, Z. Wang, Z.-Y. Ong, T. Xu, R. Xin, L. Pan, B. Wang, L. Sun, J. Wang, G. Zhang, Y.W. Zhang, Y. Shi, X. Wang, *Nat. Commun.* **5**, 5290 (2014)
29. M. Tosun, L. Chan, M. Amani, T. Roy, G.H. Ahn, P. Taheri, C. Carraro, J.W. Ager, R. Maboudian, A. Javey, *ACS Nano* **10**, 6853 (2016)
30. Y. Wan, E. Li, Z. Yu, J.-K. Huang, M.-Y. Li, A.-S. Chou, Y.-T. Lee, C.-J. Lee, H.-C. Hsu, Q. Zhan, A. Aljarb, J.-H. Fu, S.-P. Chiu, X. Wang, J.-J. Lin, Y.-P. Chiu, W.-H. Chang, H. Wang, Y. Shi, N. Lin, Y. Cheng, V. Tung, L.-J. Li, *Nat. Commun.* **13**, 4149 (2022)

31. P.-C. Shen, Y. Lin, C. Su, C. McGahan, A.-Y. Lu, X. Ji, X. Wang, H. Wang, N. Mao, Y. Guo, J.-H. Park, Y. Wang, W. Tisdale, J. Li, X. Ling, K.E. Aidala, T. Palacios, J. Kong, *Nat. Electron.* **5**, 28 (2022)
32. T. Yanase, F. Uehara, I. Naito, T. Nagahama, T. Shimada, *ACS Appl. Nano Mater.* **3**, 10462 (2020)
33. X. Zhang, Q. Liao, S. Liu, Z. Kang, Z. Zhang, J. Du, F. Li, S. Zhang, J. Xiao, B. Liu, Y. Ou, X. Liu, L. Gu, Y. Zhang, *Nat. Commun.* **8**, 15881 (2017)
34. B. Huang, F. Tian, Y. Shen, M. Zheng, Y. Zhao, J. Wu, Y. Liu, S.J. Pennycook, J.T. Thong, *ACS Appl. Mater. Interfaces* **11**, 24404 (2019)
35. S.I. Khondaker, M.R. Islam, *J. Phys. Chem. C* **120**, 13801 (2016)
36. Y. Zhang, J. Liu, Y. Pan, K. Luo, J. Yu, Y. Zhang, K. Jia, H. Yin, H. Zhu, H. Tian, *J. Mater. Sci.* **30**, 18185 (2019)
37. N. Kang, H.P. Paudel, M.N. Leuenberger, L. Tetard, S.I. Khondaker, *J. Phys. Chem. C* **118**, 21258 (2014) □

Publisher's note

Springer Nature remains neutral with regard to jurisdictional claims in published maps and institutional affiliations.



Mariam Hakami is a doctoral candidate at The University of Tokyo, Japan. She received her BS degree in physics from King Abdulaziz University, Saudi Arabia, in 2017, and her MS degree in materials science and engineering from King Abdullah University of Science and Technology, Saudi Arabia, in 2019. Her research focuses on single-crystal transition-metal dichalcogenide nanoribbons. Hakami can be reached by email at Mariam_h@chemsys.t.u-tokyo.ac.jp.



Chien-Chih Tseng is a doctoral candidate at The University of Tokyo, Japan. He received his master's degree in 2012. He was a research assistant at the National Chiao Tung University, Taiwan, for three years and materials science and engineering at King Abdullah University of Science and Technology, Saudi Arabia, for two years, respectively. His current research interest focuses on the epitaxy of graphene-like semiconducting two-dimensional materials on catalyst substrates. Tseng can be reached by email at tseng-chien-chih1982@g.ecc.u-tokyo.ac.jp.



Kohei Nanjo is a master's student at The University of Tokyo, Japan. He received his bachelor's degree in chemical systems and engineering from The University of Tokyo in 2023. His research interest focuses on the ledge-directed growth of two-dimensional materials. Nanjo can be reached by email at k_nanjo@chemsys.t.u-tokyo.ac.jp.



Vincent Tung is a professor of chemical systems and engineering at The University of Tokyo, Japan. He received his MS degree from the Department of Chemistry at the National Tsing Hua University, Taiwan, and his PhD degree from the Department of Materials Science and Engineering at the University of California, Los Angeles. He completed his postdoctoral training in the Department of Materials Science and Engineering, at Northwestern University. His research explores the epitaxial relationship between the two-dimensional epilayers and substrates. Tung can be reached by email at vincent@g.ecc.u-tokyo.ac.jp.



Jui-Han Fu is an assistant professor at The University of Tokyo, Japan. He received his PhD degree in materials science and engineering from King Abdullah University of Science and Technology, Saudi Arabia, in 2021. His current research interest focuses on the epitaxy of two-dimensional materials on arbitrary substrates. Fu can be reached by email at fu@chemsys.t.u-tokyo.ac.jp.